

CENTRALLY CONCENTRATED X-RAY RADIATION FROM AN EXTENDED ACCRETING CORONA IN  
ACTIVE GALACTIC NUCLEI

B. F. LIU,<sup>1,2</sup> RONALD E. TAAM,<sup>3,4</sup> ERLIN QIAO,<sup>1,2</sup> AND WEIMIN YUAN<sup>1,2</sup>

<sup>1</sup>*Key Laboratory of Space Astronomy and Technology, National Astronomical Observatories, Chinese Academy of Sciences, Beijing 100012, China*

<sup>2</sup>*School of Astronomy and Space Science, University of Chinese Academy of Sciences, 19A Yuquan Road, Beijing 100049, China*

<sup>3</sup>*Academia Sinica Institute of Astronomy and Astrophysics-TIARA, P.O. Box 23-141, Taipei, 10617 Taiwan; taam@asiaa.sinica.edu.tw*

<sup>4</sup>*Department of Physics and Astronomy, Northwestern University, 2131 Tech. Drive, Evanston, IL 60208, USA*

(Received July 2, 2017; Revised August 27, 2017; Accepted August 28, 2017; To appear in ApJ 847:96, 2017 Oct. 1)

ABSTRACT

The X-ray emission from bright active galactic nuclei (AGNs) is believed to originate in a hot corona lying above a cold, geometrically thin accretion disk. A highly concentrated corona located within  $\sim 10$  gravitational radii above the black hole is inferred from observations. Based on the accretion of interstellar medium/wind, a disk corona model has been proposed in which the corona is well coupled to the disk by radiation, thermal conduction, as well as by mass exchange (Liu et al. 2015; Qiao & Liu 2017). Such a model avoids artificial energy input to the corona and has been used to interpret the spectral features observed in AGN. In this work, it is shown that the bulk emission size of the corona is very small for the extended accretion flow in our model. More than 80% of the hard X-ray power is emitted from a small region confined within 10 Schwarzschild radii around a non-spinning black hole, which is expected to be even smaller accordingly for a spinning black hole. Here, the corona emission is more extended at higher Eddington ratios. The compactness parameter of the corona,  $l = \frac{L}{R} \frac{\sigma_T}{m_e c^3}$ , is shown to be in the range of 1-33 for Eddington ratios of 0.02 - 0.1. Combined with the electron temperature in the corona, this indicates that electron-positron pair production is not dominant in this regime. A positive relation between the compactness parameter and photon index is also predicted. By comparing the above model predictions with observational features, we find that the model is in agreement with observations.

*Keywords:* accretion, accretion discs – black hole physics – galaxies: active – X-rays:galaxies

arXiv:1709.09799v1 [astro-ph.HE] 28 Sep 2017

## 1. INTRODUCTION

The energetic X-ray emission from bright active galactic nuclei (AGNs) is widely believed to originate in a hot corona overlying a thin accretion disk (e.g. Vaiana & Rosner 1978; Haardt & Maraschi 1991, 1993; Nakamura & Osaki 1993; Svensson & Zdziarski 1994; Meyer et al. 2000a; Róžańska & Czerny 2000; Liu et al. 2002, 2015; Merloni & Fabian 2003). The optical–UV emission produced in the inner accretion disk is Compton up-scattered into X-rays by the hot corona. A fraction of this X-ray radiation is directly observed as a power-law component, with the remainder illuminating the disk to produce the reflection continuum and emission lines in the spectra. However, fundamental questions regarding the formation of the corona and its energizing mechanism, as well as its size and location are still under debate.

In recent years, evidence from diverse observational diagnostics points to a very compact corona located within 10 gravitational radii ( $R_g$ ) of the black hole (e.g. Reis & Miller 2013; Fabian et al. 2015). This has been deduced from the rapid variability of the 2–10 keV X-ray emission seen from many AGNs (e.g. Done & Fabian 1989) and the X-ray spectral timing studies based on reverberation analyses of AGN spectra in the scenario of "lamp post" illumination (Fabian et al. 2009; De Marco et al. 2011; Kara et al. 2013; Reis & Miller 2013; Cackett et al. 2014; Emmanoulopoulos et al. 2014; Uttley et al. 2014). Variability analyses of several lensed quasars also indicate small hard X-ray emission regions (e.g. Blackburne et al. 2006, 2011, 2014, 2015; Morgan et al. 2008, 2012; Dai et al. 2010; Mosquera et al. 2013). Further evidence for a small physical size of the corona stems from varying obscuration of the corona by clouds (Risaliti et al. 2011; Sanfrutos et al. 2013). Meanwhile, the effect of corona geometry on the emissivity profile of the broad iron line has been investigated, from which a comparison of observations and theory points to a compact X-ray emitting corona (Wilkins & Fabian 2011, 2012; Wilkins et al. 2016). Combining the observational constraints based on the inferred coronal sizes and electron temperatures, Fabian et al. (2015) studied the radiation compactness and suggested the importance of electron–positron pair production in the corona.

In contrast to the "lamp post" illumination model, Gardner & Done (2016) suggested the existence of an additional energetic emission region lying between the corona and thin disk, which produces radiation in the unobservable extreme-ultraviolet (EUV) regime. Its high-frequency tail would be seen as the "soft excess" and a low-frequency tail as a "big blue bump". Such a model was used to interpret the observed interband time lags where the EUV region serves as a reprocessor that is illuminated and heated by the X-ray corona, driving the variability in the accretion disk (Gardner & Done 2016; Edelson et al. 2017). Although the formation of such a structured component is unknown, the hard X-ray emission region/corona is very small.

On the other hand, a hybrid two-component accretion flow was proposed by Liu et al. (2015) to interpret the formation of an energetic corona and a cool, thin disk. Here, matter from the interstellar medium or from stellar winds is gravitationally captured by a supermassive black hole (e.g. Chakrabarti 1995; Ho 2008). In contrast to the case of low-mass X-ray binaries with a stellar-mass black hole, where mass is transferred from a companion star via a Roche lobe overflow, the vertically distributed interstellar medium (or stellar wind) tends to form a hot accretion flow, which partially condenses, due to the interaction between the disk and corona, to an underlying cool disk as it flows toward the black hole. Such a model leads to the existence of a strong X-ray emitting corona, which has been used to interpret the correlation between the photon index and reflection scaling factor. The best fit is obtained for a corona located above the black hole at a height of 10 Schwarzschild radii (Qiao & Liu 2017).

In this paper, we investigate the bulk emission size of the corona and its dependence on the Eddington ratio in the scenario of Liu et al. (2015). We show that the dominant emission region of the corona is indeed very small, although the hot accretion flow is quite extended. In addition, the compactness parameter is calculated, with which we find the model is self consistent since the electron–positron pair production is not important. In §2, the basic physics of the model is briefly outlined. The properties of radiation size of the corona and of the compactness parameter are presented in §3 and comparison with observations is discussed in §4. Our conclusions are presented in Section 5.

## 2. BRIEF DESCRIPTION OF THE MODEL

We consider a standard accretion disk embedded in a hot accretion flow (Liu et al. 2015). The disk and hot corona are well coupled by energy and mass exchange as a consequence of the interaction between the two-phase accretion flows. With a constant mass-supply rate the thin disk and corona can achieve a steady state, the form of which depends on the properties of the gas supplied to the accretion flow. In low-mass X-ray binaries, gas is transferred from a companion star via Roche lobe overflow and is mostly constrained in the orbital plane. Hence, accretion takes place via a thin disk in the outer region. In the inner region, evaporation is efficient, leading to the evacuation and

truncation of the thin disk if the mass-supply rate to the disk is low (e.g. Liu et al. 1999; Meyer et al. 2000b). On the other hand, if the mass-supply rate to the disk is high, evaporation is not sufficient to entirely deplete the disk at any distance. The strong emission from the disk cools the inner corona by Compton scattering, leading to a high/soft state with little coronal contribution to the X-ray emission (e.g. Meyer et al. 2000b; Meyer-Hofmeister et al. 2012). In contrast, the mass supply for accretion in AGNs results from the gravitational capture of matter from stellar winds or the interstellar medium by the central supermassive black hole. Such gas is not necessarily constrained to lie in the disk plane, and hence it can form a hot accretion flow in the outer region. This hot accretion flow, if encountering any residual thin disk, can heat the disk gas and deplete it at low mass-supply rates, similar to the case for a stellar-mass black hole. However, for a sufficiently high mass-supply rate, the hot gas condenses partially to the disk, maintaining a thin accretion disk and a strong corona close to the black hole. Such a strong corona is essential for the interpretation of the strong X-ray emission observed in bright AGNs (Liu et al. 2015; Qiao & Liu 2017). The physical mechanisms involved in the disk corona interaction are similar in both the black hole X-ray binary systems (BHXRBS) and AGN. The relative strength of the two-phase accretion flow in BHXRBS and AGNs reflects the differing properties of the mass supply. A continuous supply of matter to the accreting corona in AGNs provides for strong X-ray radiation, even if condensation of coronal gas is efficient. Such a model avoids artificial energy input and gas supplement to the corona, which are the necessary assumptions in previous models, but which remain to be clarified.

Details of the disk corona interaction processes and relevant equations can be found in Liu et al. (2015) and Qiao & Liu (2017). The resultant accretion flows appear somewhat similar to the two-component model developed by Chakrabarti & Titarchuk (1995); however, the interaction processes between the cold and hot flows, and boundary condition in our model significantly differ. Specifically, we adopt a hot, geometrically thick flow (Narayan & Yi 1994) fed by the AGN environment, without an unstable self-gravitating region in the thin disk. Such an accretion flow partially condenses into a residual disk in the innermost radial regions as a consequence of mass and radiative coupling between the hot accretion flow and the cool disk (Liu et al. 2015). The steady condensation of a hot accretion flow feeds an inner thin disk, which is different from a large disk fed by the Roche lobe overflow process in the stellar-mass black hole context. The model of Chakrabarti & Titarchuk (1995) posits a Keplerian optically thick flow in the disk midplane and a sub-Keplerian optically thin flow near the disk surface with the viscosity parameter decreasing with disk height. Provided that the viscosity in the hot optically thin halo region is sufficiently low, shock waves can form in the halo. On the other hand, in our model, based on a large viscosity parameter which is constant throughout the corona, such shock waves are not present. Therefore, our boundary condition (gas supply), the geometry of the accretion flow (ADAF-like hot flow and passive disk), and the physics of interaction between the disk and corona are significantly different from the model of Chakrabarti & Titarchuk (1995).

With the same assumption and method as that of Liu et al. (2015) and Qiao & Liu (2017), we study the energy balance involving thermal conduction and Comptonization, and calculate the coronal temperature, density, and mass-exchange rate between the disk and the corona. The calculations are iterative because illumination by the corona emission and the mass-exchange rate are involved in determining the coronal property. The main computational results for the radiation spectrum have been presented in Liu et al. (2015) and Qiao & Liu (2017). In the following, we investigate the radiation compactness and discuss the model predictions with respect to the observations.

### 3. COMPUTATIONAL RESULTS

The basic model parameters include the mass of a non-rotating black hole,  $M$ , the Eddington-scaled accretion rate,  $\dot{m}$ , the viscosity parameter,  $\alpha$ , and the magnetic field as measured by the ratio of gas pressure to total pressure,  $\beta$ . In calculating the coronal property, illumination from the corona contributes to the seed photons in addition to the accretion disk photons for Comptonization. For this purpose, we adopt a lamp post illumination from a height of 10 Schwarzschild radii ( $R_S$ ) and albedo  $a = 0.15$ . This height is justified by the comparison of the model prediction with the observed reflection scaling factor (Qiao & Liu 2017), and it is roughly consistent with the size of the bulk emission region as shown in the following section. Given  $M = 10^8 M_\odot$ ,  $\alpha = 0.3$ , and  $\beta = 0.95$ , the emission and spectra for  $\dot{m} = 0.02, 0.03, 0.05$ , and  $0.1$  are calculated.

#### 3.1. Size of the Dominant Emission Region

We integrate the coronal radiation power from the innermost stable circular orbit (ISCO) to a distance  $R$ , and calculate the ratio of this luminosity to the total coronal luminosity,  $L(R)/L_{\text{tot}}$ . Such a ratio represents the fraction of cumulative luminosity emitted from the region within  $R$ , which is used to determine the size of coronal emission

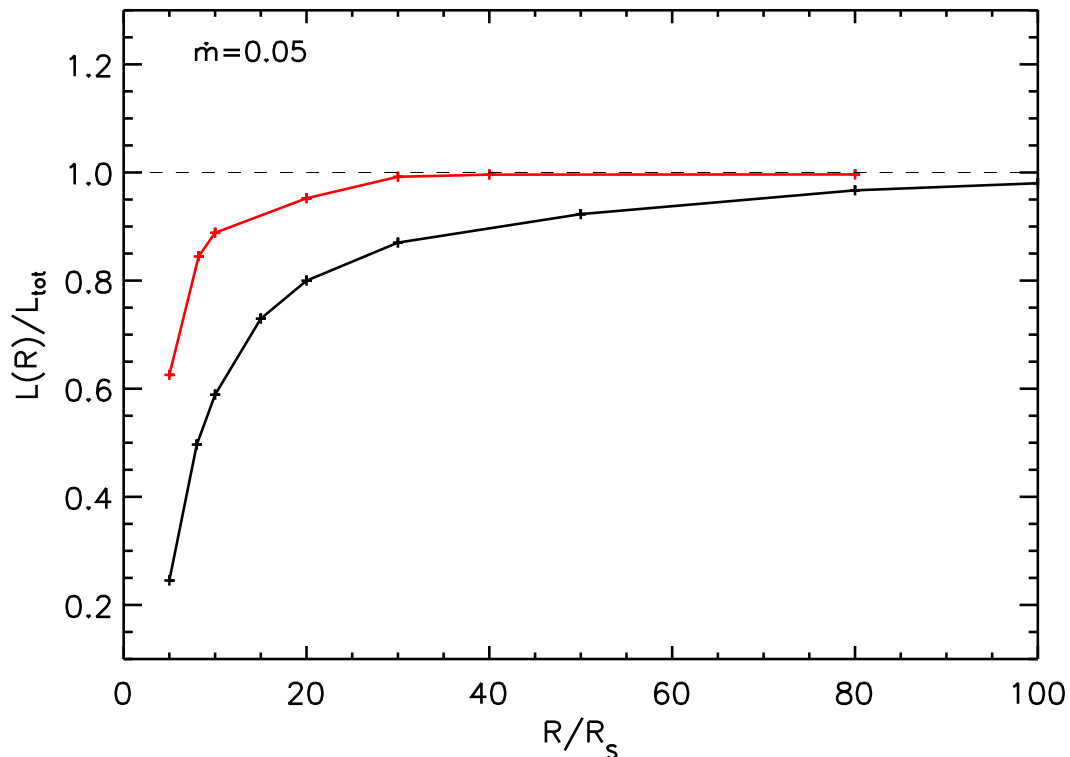


**Figure 1.** Cumulative radiation fraction of the total emission (lower curve) and hard X-ray emission (upper curve) from the corona as a function of radius in units of the Schwarzschild radius. More than 80% of the hard X-ray luminosity is emitted from the inner region within  $10R_S$ . The difference between hard X-ray and total corona radiation indicates that the hard X-ray radiation region is more compact than the region emitting soft X-ray radiation.

region. For a typical accretion rate,  $\dot{m} = 0.05$ , the corona luminosity contributed by different regions as compared with total corona luminosity,  $L(R)/L_{\text{tot}}$ , is illustrated in Figure 1. For comparison, we also plot the hard X-ray ( $2 - 10\text{keV}$ ) luminosity contribution. It can be seen that more than 80% of the corona emission is contributed from the inner region  $R \leq 20R_S$ . The hard X-ray emission is from a more concentrated region, as more than 80% of the hard X-ray luminosity is emitted from the inner region within  $10R_S$ , and nearly all from within  $30R_S$ . This implies that the source of hard X-ray radiation is smaller than the soft X-ray radiation as measured by the bulk emission. In the following sections, the radial distribution of the total corona radiation is used as a probe of the corona radiation size. Such an emission size can be converted to the height of a point-like illumination source above the disk within the interpretative framework of lamp post illumination picture (see Section 4). Because the hard X-ray emission is contributed from a smaller region as illustrated in Fig.1, the size of the bulk emission region calculated from total corona emission is larger than that deduced from hard X-ray reverberation analysis.

The luminosity fraction from the radial regions is calculated for mass-supply rates of  $\dot{m} = 0.02, 0.03, 0.05$ , and  $0.1$ . In Fig.2, the distributions for all the accretion rates (left panel) and the size of the emitting region as a function of Eddington ratio (right panel) are plotted. It can be seen that the bulk of the luminosity originates from a more extended region at a higher Eddington ratio (or accretion rate). This result can be understood from the radial distribution of the coronal accretion rate for different mass-supply rates, as shown in Liu et al. (2015) and Qiao & Liu (2017). For a higher mass-supply rate, the accretion rate in the inner corona increases more steeply with distance as a consequence of the stronger condensation (see Fig.2 in Qiao & Liu 2017). Therefore, the energy release through accretion is more extended at higher mass-supply rates.

Within our model assumptions, the above computational results are obtained for a non-spinning black hole. We note that the size of bulk emission region should be systematically smaller for a rapidly rotating black hole since the accretion flow can extend closer to the event horizon.

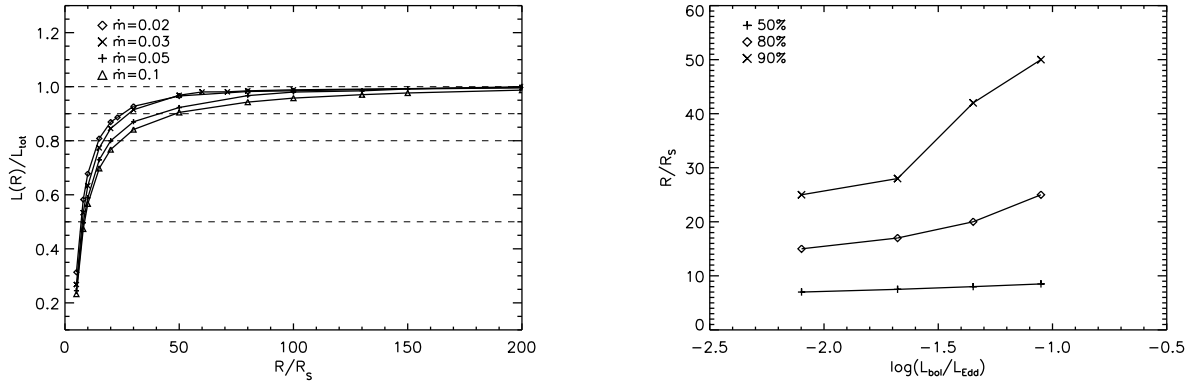


**Figure 2.** Left: the radial distribution of the cumulative radiation fraction of the corona for a range of mass accretion rates; the coronal emission is more extensive at higher accretion rates. Right: the size of emitting region as a function of the Eddington ratio. Fifty percent of the coronal luminosity is contributed from a region smaller than  $10R_s$  for different Eddington ratios; 80% of the luminosity is emitted from  $R < 15R_s$  for Eddington ratio  $\sim 8 \times 10^{-3}$ . For the same luminosity fraction, the contributed region is larger for a higher Eddington ratios. This trend is consistent with observation (e.g. Fig.7 of Kara et al 2016), though the range of our Eddington ratio is small.

### 3.2. Radiation Compactness of the Corona

For a self-consistent examination of our model and comparison of the model prediction with observations, we also calculate the traditional compactness parameter (Guilbert et al. 1983)

$$l = \frac{L}{R} \frac{\sigma_T}{m_e c^3} \quad (1)$$

where  $R$  is the radius of a spherical source,  $L$  is the luminosity produced within the source,  $\sigma_T$  is the Thomson cross-section, and  $m_e$  is the mass of the electron. This compactness parameter is a measure of the importance of coronal cooling as it represents the ratio of the corona cooling time to the light-crossing time. If the emitting photons are sufficiently energetic,  $h\nu \gtrsim m_e c^2$ , photon–photon collisions can lead to the creation of electron–positron pairs. The probability of the pair production can also be measured by the compactness parameter. If  $l$  reaches a certain value, a significant fraction of the source luminosity is lost in pairs and is then reradiated at lower energies, which can play a major role in determining the outgoing spectrum and overall composition of the corona (e.g. Svensson 1984).

For an optically thin corona, the radiation luminosity  $L$  is approximately given by the sum of emission from the entire region,

$$L = \frac{4}{3} \pi R^3 q_c, \quad (2)$$

where  $q_c$  is the radiation cooling rate per unit volume in the corona, i.e., the emissivity of the corona. The cooling time of the corona can then be expressed as

$$t_c = \frac{n_e \gamma m_e c^2}{q_c}, \quad (3)$$

where  $\gamma = 1/\sqrt{1 - v^2/c^2}$  the Lorentz factor and  $n_e$  the number density of the electrons. Combining Eqs.(1)–(3) and using the definition of the scattering optical depth  $\tau = n_e \sigma_T R$ , we derive the cooling time of the corona compared to light-crossing time as

$$\frac{t_c}{R/c} = \frac{\frac{4}{3} \pi \gamma \tau}{l}, \quad (4)$$

The above expression (Eq.4) is independent of the radiation mechanism and is valid for an optically thin corona. The detailed radiation processes are implicitly included in the compactness parameter  $l$  through the luminosity. Eq.(4) reveals the physical meaning of compactness parameter  $l$  as follows. For a corona with typical value  $\tau \sim 0.5$ , if the electrons are non-relativistic,  $\gamma \approx 1$ , an electron is cooled by radiation in a light-crossing time when  $l \approx 2$ . A larger value of  $l$  indicates the more rapid cooling of electrons with its timescale shorter than the light-crossing time.

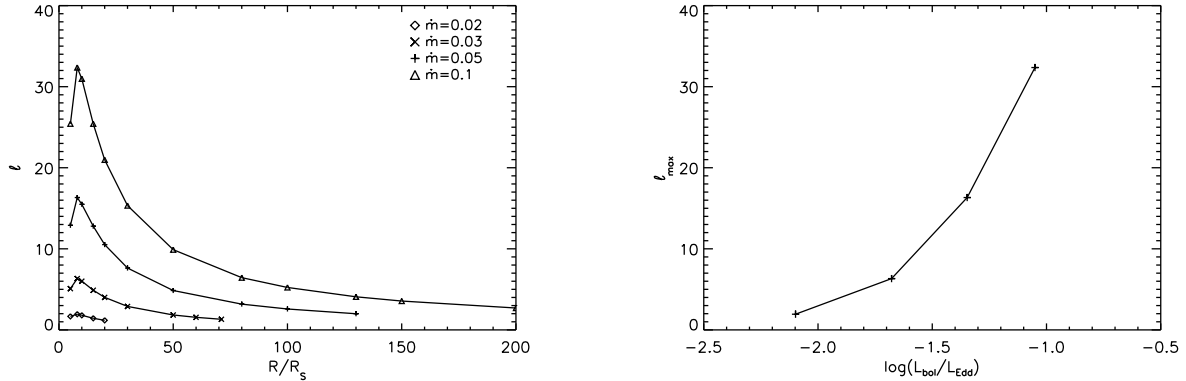


**Figure 3.** Left: the radial distribution of the compactness parameter  $l$  for mass-supply rates  $\dot{m} = 0.02, 0.03, 0.05, 0.1$ . Right: the dependence of the maximal compactness parameter  $l_{\max}$  on Eddington ratio.

Note that Eq.(4) does not imply that radiative cooling is slow for energetic electrons or for high-scattering depth. In fact, the radiation power of a relativistic electron is proportional to  $\gamma^2$ , independent of whether the emission is from inverse Compton scattering or synchrotron radiation. Energetic electrons produce stronger radiation,  $l \propto L \propto \gamma^2$ , thereby leading to a shorter cooling time as compared to a light-crossing time,  $\frac{t_c}{R/c} \propto 1/\gamma$ . This effect is significant for ultra-relativistic electrons. The scattering optical depth also affects the radiation compactness. A large scattering depth in a given region (fixed  $R$ ) corresponds to a high-electron density, leading to a high total radiation power by either synchrotron or Compton radiation. Thus, the radiation is more compact for larger  $\tau$ . For ultra-relativistic electrons this effect is not as significant as the Lorentz factor  $\gamma$ , as  $\tau$  is not much less than 1 in the optically thin corona, as required by the observed bright X-ray emission in AGN. The emission power from synchrotron radiation or inverse Compton scattering of external photons is proportional to  $n_e$ , which cancels  $n_e$  contained in  $\tau$  in Eq.(4). Thus, the ratio of cooling time to light-crossing time is independent of the electron density. For the Synchrotron Self Compton (SSC) process, where electrons take part in both the synchrotron process and Compton scattering, the emission power is  $\propto n_e^2$ . For Bremsstrahlung radiation, the radiation power is similar to SSC,  $\propto n_e n_i \propto n_e^2$ . In these cases, we have  $\frac{t_c}{R/c} \propto 1/\tau$ , indicating a longer cooling time compared with the light-crossing time for lower densities. Such a case usually occurs at low Eddington-scaled accretion rates where external Compton scattering is unimportant compared to SSC or Bremsstrahlung in an optically thin corona or ADAF.

To summarize, the radiation compactness parameter,  $l$ , is very large for relativistic electrons. For a thermal corona, this signifies a high temperature. With the decrease of temperature, electrons are non-relativistic and the radiation compactness parameter is smaller. The compactness in a thermal corona also depends on the scattering depth, which is reflected in the Eddington-scaled accretion rate in the corona. At a high accretion rate, the radiation is strong and  $l$  is large. When the accretion rate is very low, and SSC or Bremsstrahlung is the dominant cooling process, the corona radiation is no longer strong and hence  $l$  is small, as that in an ADAF.

We calculate the compactness parameter of the corona and plot  $l-r$  in Fig. 3 for the mass-supply rates corresponding to  $\dot{m} = 0.02, 0.03, 0.05$ , and  $0.1$ . It can be seen that the compactness parameter increases with decreasing radius as the flux from the seed photons increases, reaching its maximum at about  $8R_s$  and then decreasing again as a combination of the Compton  $y$ -parameter and the density of seed photons near the ISCO decreases. The value of  $l$  ranges from 1 to 33 and is less than 10 in the outer region with  $R > 50R_s$  in the range of the calculated accretion rates. Taking the maximum compactness parameter as an estimate of the compactness of the inner region for each accretion rate, in Figure 3 we plot the value of  $l_{\max}$  versus the Eddington ratio, where the Eddington ratio is calculated from the spectral energy distribution for a given accretion rate. This figure demonstrates that the coronal compactness parameter is larger for higher Eddington ratios, indicating stronger radiation in the corona.

At very high compactness, photon-photon collisions are efficient, leading to electron-positron pair production if a large fraction of the coronal emission is in the high-energy band,  $h\nu \sim m_e c^2$ . In an optically thin thermal corona, the inverse Compton scattering of the soft photons produces a power-law radiation spectrum extending to a Wien tail at energies  $h\nu \sim 2kT_e$  (Petrucci et al. 2001), which is  $3kT_e$  in the case of saturated scattering (Rybicki & Lightman 1979). For the disk corona model considered here, the electron temperatures are  $\sim 10^9\text{K}$ , corresponding to a high-

energy cutoff  $h\nu \sim 0.3m_e c^2$ . This suggests that the high-energy  $\gamma$ -ray photons are only a small fraction of the total coronal emission. Even if the model parameters are adjusted to produce a flat spectrum in the energy range 2-10keV, the number density of  $\gamma$ -ray photons cannot be very high in the thermal corona. This is in contrast to the case for non-thermal emission, in which a large fraction of  $\gamma$ -rays could be expected; in particular, in the case where a flat X-ray spectrum is observed.

As the coronal temperature sets an upper limit for the radiation tail of the corona, the probability of pair production caused by collisions of high-energy photons depends on the electron temperature. Detailed radiative transfer calculations including both the energy and pair balance yield a critical value of  $l$  as a function of electron temperature, which depends on the geometry (Svensson 1984, 1996; Stern et al. 1995). The most stringent constraint to the upper limit for  $l$  in the "pair-free" regime is for slab geometry (see Fig.3 in Svensson 1996). Our calculations, based on the assumption that radiation originates from inverse Compton scattering, synchrotron, and bremsstrahlung processes, yield values of  $l$  marginally below the critical value given by Stern et al. (1995) or Svensson (1996). At higher accretion rates beyond our calculations, we expect stronger coronal radiation, which leads to a larger compactness parameter  $l$ . However, the electron temperature should slightly decrease as a consequence of more efficient Compton cooling, which alleviates the importance of pair production. Hence, pair production is not expected to significantly affect the emergent radiation, indicating that our model is self consistent.

#### 4. DISCUSSION

X-ray reverberation provides a new technique for investigating the geometry of the accretion flow in the inner region of an accretion disk surrounding a supermassive black hole. Observations using the *XMM-Newton* and *NuSTAR* satellites have shown that the soft X-ray excess (Fabian et al. 2009; De Marco et al. 2013; Reis & Miller 2013), broad iron  $K$  line (Zoghbi et al. 2012; Kara et al. 2013, 2016), and Compton hump (Zoghbi et al. 2014; Kara et al. 2015) all lag the continuum emission. This time lag is assumed to be caused by the light-travel time between the corona and the ionized accretion disk, providing a probe of the height and extent of the coronal source. Along this line of investigation, significant efforts have been directed toward observationally constraining the corona geometry. It is found that the coronal illumination may originate from a height less than  $10R_g$  (Detailed data analyses on the reverberation lag and deduced height of the corona can be found in Fabian et al. 2009, 2015; De Marco et al. 2013; Kara et al. 2013, 2015, 2016; Reis & Miller 2013).

As a hot accretion flow, the vertical extent of the corona at any distance is approximately equal to the radius. If the illumination from the corona is approximated as a point source, as adopted in phenomenological models, the average height of illumination should be less than half of the radial extent ( $R_{\text{out}}$ ) of bulk emission region, as estimated from

$$\langle H \rangle = \frac{1}{L} \int_{R_{\text{ISCO}}}^{R_{\text{out}}} \frac{H}{2} \frac{dL}{dR} dR = \frac{1}{4} (R_{\text{out}} + R_{\text{ISCO}}) < \frac{1}{2} R_{\text{out}}, \quad (5)$$

where homogeneous radiation in coronal annuli (i.e.  $\frac{dL}{dR} = \text{constant}$ ) and  $H = R$  are assumed. Taking into account of the radially decreasing coronal luminosity of  $\frac{dL}{dR}$ , the location of an illumination source should be smaller than the approximation given in Eq.(5). In §3, it was demonstrated that the coronal radiation is, indeed, concentrated in the inner region. For example, the radial extent is  $\sim 10R_g$  and  $\sim 5R_g$  corresponding to 80% and 60% of the hard X-ray luminosity respectively for  $\dot{m} = 0.05$ , implying the bulk emission is respectively from a region smaller than  $\sim 5R_g$  and  $\sim 2.5R_g$ . This suggests that the disk corona model adopted here is roughly consistent with the observations.

Kara et al. (2016) carried out a survey of the X-ray time lags in a large sample of Seyfert galaxies observed with *XMM-Newton* and found that the coronal source height tends to be larger for sources at higher Eddington ratios, though there is large scatter (in their Fig. 7 and Fig. 8). This is consistent with the theoretical expectation that the size of the bulk emission region is a function of the Eddington ratio (right panel in Figure 2).

Additional observational support for this correlation is provided by the work of Gallo et al. (2015) on the narrow-line Seyfert galaxy Mrk 335. Here, deep X-ray observations of this galaxy in the low-flux state when combined with observations of the source when it was in a state 10 times brighter showed that the scenario of blurred reflection from an accretion disk (e.g. Ross & Fabian 2005) is more likely than the partial-covering absorption scenario (e.g. Tanaka et al. 2004) based on both long-term and rapid variability. Adopting the reflection model, Gallo et al. (2015) found that the high-flux state of Mrk 335 is consistent with continuum-dominated, jet-like emission, of which the ejecta is confined and bound to within  $\sim 25R_g$ . On the other hand, the corona becomes compact, extending to only  $5R_g$  from the black hole during the low flux state, with its spectrum dominated by the reflection component. Keek & Ballantyne (2016)

performed a multi-epoch spectral analysis of all *XMM-Newton*, *Suzaku*, and *NuSTAR* observations of Mrk 335. The low-flux state was interpreted as a compact and optically thick corona, which is located close to the inner disk, whereas in the high-flux state the corona is optically thin and extends vertically further away from the disk. Although the presumed coronal geometry differs from our model, these results point to the same conclusion that the corona is more extended at a higher Eddington ratio.

The above observational features can be understood as a consequence of the disk corona interaction. At low mass-supply rates, the coronal gas can remain in the corona without significant condensation. Thus, the radial distribution of the accretion rate in the corona is flat. The corona radiation is concentrated in the innermost region where there is a greater release of radiation than in the outer region. This innermost region corresponds to a very small height ( $H < R/2$ ) when it is approximated as a point source. At a high mass supply rate, gas condenses to the disk, leading to a stronger disk. This, in turn, boosts coronal cooling through external Compton scattering and, hence, enhances gas condensation in the inner region, resulting in a steep radial distribution of the accretion rate in the corona and extended radiation. The illumination flux to the innermost disk (where most of the blurred Fe lines are produced) depends on the location of the illumination source and is given by

$$F_{\text{il}} = \frac{L_{\text{il}}}{4\pi} \frac{H}{(R^2 + H^2)^{3/2}} \propto \frac{L_{\text{il}}}{R^2}, \quad (6)$$

where  $L_{\text{il}}$  is the luminosity of a point source located at a radius of  $R$  and a height of  $H \sim R$ . Hence, the radiation from the innermost corona plays a key role in affecting the reflection component, as a consequence of the distance-dependent illumination flux. The strength of the reflection relative to the direct emission increases with the fraction of luminosity from the innermost region of the corona. As shown in Figure 2, the luminosity is distributed more extensively at a high Eddington ratio, leading to the expectation that reflection is less important. In this sense, it is not necessary to introduce an outflowing corona at high Eddington ratios. The change in the geometry of the corona can be interpreted as a smooth variation in the hot corona and the thin disk as a function of the mass-supply rate to the accretion flow. More detailed computations with a radially distributed illumination in the scenario of the condensation model is required for quantitative comparison with observations.

The illumination of a disk from a corona for various geometries (i.e., a point source, a radially extended slab corona, a vertically extended cylindrical corona, and a collimated outflow) has been investigated to determine the X-ray reflection emissivity profiles based on general relativistic ray-tracing simulations (Wilkins & Fabian 2011, 2012; Wilkins et al. 2016). Combined with the observed reverberation time lags, Wilkins & Fabian (2012) fitted the broadened iron  $K$  emission line in the spectrum of 1H 0707-495 and found an extended region of primary X-ray emission located as low as  $2R_g$  above the accretion disk, extending outwards to a radius of around  $30R_g$ . Although the geometry is simple and the extended corona is homogeneous, these investigations provide a constraint on the geometry of the illumination source. Given that the corona emission is inhomogeneous and the scale height varies with distance in our model, the X-ray reflection emissivity is expected to differ from these simplified models.

Kara et al. (2015, 2016) point out that the true light-travel time between the corona and the disk is longer than the observed lag measured by X-ray reverberation due to dilution effects. The direct emission from the corona, as our model reveals, unavoidably contributes a fraction to the reflection band. This part, as the leading variation component, will dilute the lag of the reflected component. When converting the observed lag into a distance, the correction factor associated with the dilution effect is dependent on the relative contribution of the direct emission in the reflection band and can lead to an upward revision of the distance by a factor up to 4 (Kara et al. 2015). For example, the dilution to the reflection component in the soft X-ray band ( $< 1\text{keV}$ ) is stronger than that for the iron  $K$  line band. As a consequence, the true size of the corona could be a few times larger than the values derived from reverberation. By taking the dilution effect into account, the radiation size deduced from the observations would be in better agreement with that predicted by the corona condensation model.

In addition to constraints imposed by variability, micro-lensing is another potential tool for estimating the emission size of the corona. Observations of lensed quasars have shown that the half-light radius of the hard X-ray emission region is  $20R_g$  for PG 1115+080 (Morgan et al. 2008),  $\lesssim 16R_g$  for QJ 0158-4325 (Morgan et al. 2012),  $\approx 20R_g$  for Q 2237+0305 (Mosquera et al. 2013),  $\sim 10R_g$  for HE 0435-1223 (Blackburne et al. 2014),  $25R_g$  for HE 1104-1805 (Blackburne et al. 2015), and  $< 24R_g$  for J 0924+0219 (MacLeod et al. 2015). These measurements, as listed in Table 1, constrain the quasar X-ray emission size to be  $\sim 20R_g$  (see also Blackburne et al. 2006; Pooley et al. 2006; Chartas et al. 2009; Dai et al. 2010). Chen et al. (2011) and Mosquera et al. (2013) detected energy-dependent X-ray



micro-lensing in Q 2237+0305, suggesting that the hard X-ray component is more compact than the soft one. The size of bulk X-ray emission predicted by the condensation model is roughly consistent with micro-lensing observations, as shown in Fig.1 where it can be seen that the hard X-ray component is more compact than the soft X-ray component.

**Table 1.** The Half-light Radius of the Hard X-ray Emission Region for Micro-lensed AGN

Source	$\log R(\text{cm})$	$M/M_{\odot}$	Reference	$R/R_g$
PG 1115+080	$15.6^{+0.6}_{-0.9}$	$1.2 \times 10^9$	Morgan et al. 2008	20
Q J0158-4325	$\lesssim 14.6$	$1.6 \times 10^8$	Morgan et al. 2012	$\lesssim 16$
Q 2237+0305	15.46	$\approx 10^9$	Mosquera et al. 2013	$\approx 20$
HE 0435-1223	$< 14.8$	$\gtrsim 5 \times 10^8$	Blackburne et al. 2014	$\sim 10$
HE 1104-1805	15.33	$5.9 \times 10^8$	Blackburne et al. 2015	25
J 0924+0219	$< 15$	$2.8 \times 10^8$	MacLeod et al. 2015	$< 24$

As remarked in §3, the value of the compactness parameter  $l$  measures the importance of radiation cooling on the light-crossing time, revealing the importance of the pair production process operating in the corona. The value predicted by our model ranges from 1 to 33, which indicates strong emission in the inner corona. The electron temperatures in the region with maximal compactness parameter are  $\sim 10^9\text{K}$ . Thus, the value of  $l$  is marginally below the critical value for the pair production to affect the spectrum, suggesting that the inverse Compton scattering, synchrotron and bremsstrahlung emission can be regarded as the dominant cooling processes in our model.

This differs somewhat from the conclusion of Fabian et al. (2015), who examined the compactness parameter  $l$  for a collection of objects. In their study, the coronal sizes were based on the modeling of the reflection spectrum, measurements by X-ray reverberation or by micro-lensing analysis. If no measurement existed a value of  $10R_g$  was adopted. The derived compactness  $l$  values are mostly below 100, but are systematically larger than the values predicted by the condensation model. If the dilution effect in reverberation measurements were taken into account, they can be expected to be more consistent. On the other hand, Fabian et al. (2015) point out that the general relativistic effects associated with the gravitational redshift and light-bending can boost the intrinsic values of  $l$  by factors of around 2-10 above the observed estimates. However, such an effect is predicated under the assumption of an extremely small corona. If the corona size/height is not as small as  $10R_g$ , as our model predicts, or as observationally inferred with dilution taken into account, the contribution due to general relativistic effects could be overestimated. Additionally, the radial extent of the corona is larger than the vertical height deduced from reverberation lags, as discussed above. If this effect is considered, the value of  $l$  in Fabian et al. (2015) is closer to that predicted by the disk corona model. This suggests that the pair production may not be the dominant process in cooling and heating of the corona, though it may be involved.

To compare with observation, we illustrate the relation between the maximal compactness parameter ( $l_{\text{max}}$ ) and the 2-10keV photon index ( $\Gamma$ ) in Fig.4. As both the compactness parameter and the photon index increase with Eddington ratio, a positive correlation between these properties is expected, as shown in Figure 4. Although the the curve of  $l_{\text{max}} - \Gamma$  only covers a small range in both the compactness parameter and photon index, it is close to the curve derived for a slab corona and below the curve for a hemispheric corona in energy and pair balance (Stern et al. 1995). However, the compactness parameter for given  $\Gamma$  is systematically smaller than the data shown in Fig.8 of Fabian et al. (2015), which could be caused by different size of radiation region as discussed above.

## 5. CONCLUSION

The bulk emission size of the corona and its radiation compactness are investigated on the basis of the corona condensation model (Liu et al. 2015; Qiao & Liu 2017). It is found that the emission region is small in spite of a radially extended corona flow. The hard X-ray emission is contributed by an even smaller region than that of the soft X-rays, as measured by the bulk emission from the corona. Specifically, more than 80% of the hard X-ray luminosity is emitted from a region less than  $10R_S$ , comparing favorably with micro-lensing measurements. Combining the radial distribution of coronal emission and the assumption of a geometrically thick corona in the model, we show that the height of a point-like illumination source in the lamp post model should be smaller than half of the radial size of the bulk emission. This implies that the illumination height is roughly in agreement with that deduced from reverberation

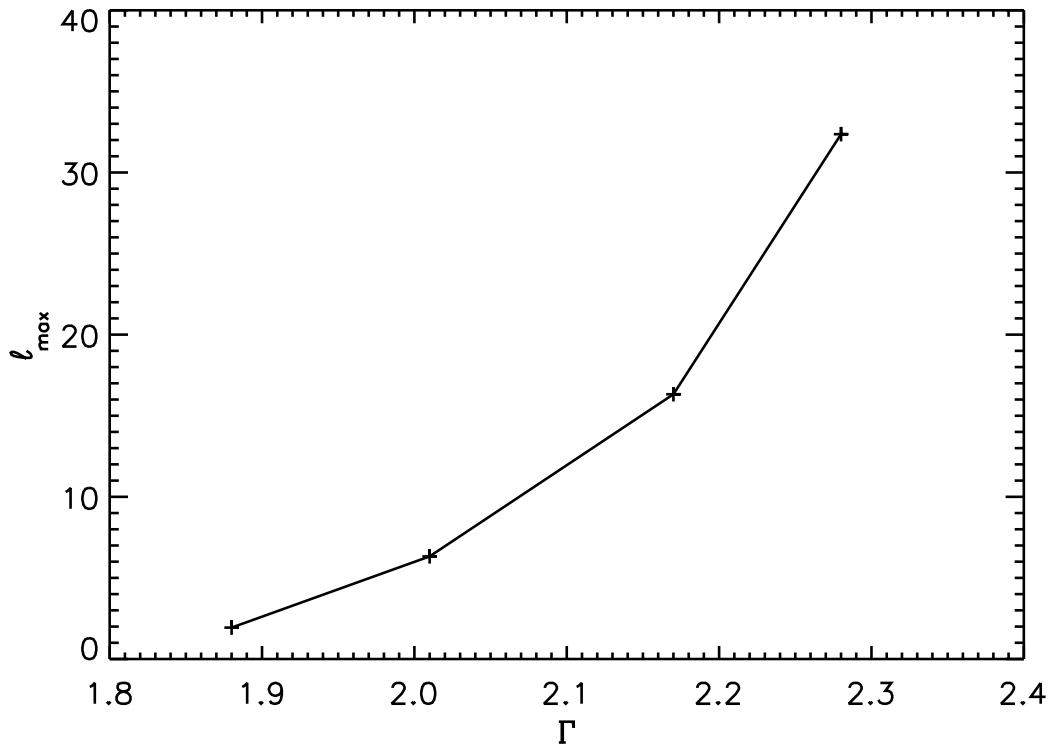


**Figure 4.** Dependence of the maximal compactness parameter  $l_{\max}$  on photon index  $\Gamma$  in 2-10keV energy band.

time lag measurements. At lower accretion rates/Eddington ratios, the model predicts an even smaller region of bulk emission, which is also consistent with the purported correlation found in the observations.

The traditional compactness parameter has been calculated to estimate the radiation cooling timescale as compared to the light-crossing timescale. The compactness parameter ranges from 1 to 33 for mass accretion rates from 0.02 to 0.1, respectively. Combined with the electron temperatures given by the model, we find that the value of the compactness parameter is marginally below the critical value for the dominance of electron-positron pair production. Therefore, the disk corona model is self consistent. Finally, a positive relation between the compactness parameter and photon index is also predicted by the model.

The calculations presented here are restricted to Eddington ratios up to 0.1 given the upper limit for the accretion flow in a stable ADAF. As such, our models do not address the strong corona inferred from observations of sources at high Eddington ratios. With vertical heat conduction and Compton scattering of strong disk photons, the upper limit for the accretion rate in a stable corona can differ from that of an ADAF. Investigations under which a strong corona can exist at higher Eddington ratio are planned for the future.

Financial support for this work was provided by the National Program on Key Research and Development Project (grant No. 2016YFA0400804) and the National Natural Science Foundation of China (grant 11673026). In addition, R.E.T. acknowledges support from the Theoretical Institute for Advanced Research in Astrophysics in the Academia Sinica Institute of Astronomy & Astrophysics.

#### REFERENCES

- Blackburne, J. A., Kochanek, C. S., Chen, B., Dai, X., & Chartas, G. 2014, *ApJ*, 789, 125
- Blackburne, J. A., Pooley, D., & Rappaport, S. 2006, *ApJ*, 640, 569
- . 2015, *ApJ*, 798, 95

- Blackburne, J. A., Pooley, D., Rappaport, S., & Schechter, P. L. 2011, *ApJ*, 729, 34
- Cackett, E. M., Zoghbi, A., Reynolds, C., et al. 2014, *MNRAS*, 438, 2980
- Chakrabarti, S., & Titarchuk, L. G. 1995, *ApJ*, 455, 623
- Chakrabarti, S. K. 1995, *ApJ*, 441, 576
- Chartas, G., Kochanek, C. S., Dai, X., Poindexter, S., & Garmire, G. 2009, *ApJ*, 693, 174
- Chen, B., Dai, X., Kochanek, C. S., et al. 2011, *ApJL*, 740, L34
- Dai, X., Kochanek, C. S., Chartas, G., et al. 2010, *ApJ*, 709, 278
- De Marco, B., Ponti, G., Cappi, M., et al. 2013, *MNRAS*, 431, 2441
- De Marco, B., Ponti, G., Uttley, P., et al. 2011, *MNRAS*, 417, L98
- Done, C., & Fabian, A. C. 1989, *MNRAS*, 240, 81
- Edelson, R., Gelbord, J., Cackett, E., et al. 2017, *ApJ*, 840, 41
- Emmanoulopoulos, D., Papadakis, I. E., Dovčiak, M., & McHardy, I. M. 2014, *MNRAS*, 439, 3931
- Fabian, A. C., Lohfink, A., Kara, E., et al. 2015, *MNRAS*, 451, 4375
- Fabian, A. C., Zoghbi, A., Ross, R. R., et al. 2009, *Nature*, 459, 540
- Gallo, L. C., Wilkins, D. R., Bonson, K., et al. 2015, *MNRAS*, 446, 633
- Gardner, E., & Done, C. 2016, *ArXiv e-prints*, arXiv:1603.09564
- Guilbert, P. W., Fabian, A. C., & Rees, M. J. 1983, *MNRAS*, 205, 593
- Haardt, F., & Maraschi, L. 1991, *ApJL*, 380, L51
- . 1993, *ApJ*, 413, 507
- Ho, L. C. 2008, *ARA&A*, 46, 475
- Kara, E., Alston, W. N., Fabian, A. C., et al. 2016, *MNRAS*, 462, 511
- Kara, E., Fabian, A. C., Cackett, E. M., et al. 2013, *MNRAS*, 428, 2795
- Kara, E., Zoghbi, A., Marinucci, A., et al. 2015, *MNRAS*, 446, 737
- Keek, L., & Ballantyne, D. R. 2016, *MNRAS*, 456, 2722
- Liu, B. F., Mineshige, S., Meyer, F., Meyer-Hofmeister, E., & Kawaguchi, T. 2002, *ApJ*, 575, 117
- Liu, B. F., Taam, R. E., Qiao, E., & Yuan, W. 2015, *ApJ*, 806, 223
- Liu, B. F., Yuan, W., Meyer, F., Meyer-Hofmeister, E., & Xie, G. Z. 1999, *ApJL*, 527, L17
- MacLeod, C. L., Morgan, C. W., Mosquera, A., et al. 2015, *ApJ*, 806, 258
- Merloni, A., & Fabian, A. C. 2003, *MNRAS*, 342, 951
- Meyer, F., Liu, B. F., & Meyer-Hofmeister, E. 2000a, *A&A*, 361, 175
- . 2000b, *A&A*, 354, L67
- Meyer-Hofmeister, E., Liu, B. F., & Meyer, F. 2012, *A&A*, 544, A87
- Morgan, C. W., Kochanek, C. S., Dai, X., Morgan, N. D., & Falco, E. E. 2008, *ApJ*, 689, 755
- Morgan, C. W., Hainline, L. J., Chen, B., et al. 2012, *ApJ*, 756, 52
- Mosquera, A. M., Kochanek, C. S., Chen, B., et al. 2013, *ApJ*, 769, 53
- Nakamura, K., & Osaki, Y. 1993, *PASJ*, 45, 775
- Narayan, R., & Yi, I. 1994, *ApJL*, 428, L13
- Petrucci, P. O., Haardt, F., Maraschi, L., et al. 2001, *ApJ*, 556, 716
- Pooley, D., Blackburne, J. A., Rappaport, S., Schechter, P. L., & Fong, W.-f. 2006, *ApJ*, 648, 67
- Qiao, E., & Liu, B. F. 2017, *MNRAS*, 467, 898
- Reis, R. C., & Miller, J. M. 2013, *ApJL*, 769, L7
- Risaliti, G., Nardini, E., Elvis, M., Brenneman, L., & Salvati, M. 2011, *MNRAS*, 417, 178
- Ross, R. R., & Fabian, A. C. 2005, *MNRAS*, 358, 211
- Rózańska, A., & Czerny, B. 2000, *MNRAS*, 316, 473
- Rybicki, G. B., & Lightman, A. P. 1979, *Radiative processes in astrophysics*
- Sanfrutos, M., Miniutti, G., Agís-González, B., et al. 2013, *MNRAS*, 436, 1588
- Stern, B. E., Poutanen, J., Svensson, R., Sikora, M., & Begelman, M. C. 1995, *ApJL*, 449, L13
- Svensson, R. 1984, *MNRAS*, 209, 175
- . 1996, *A&AS*, 120, 475
- Svensson, R., & Zdziarski, A. A. 1994, *ApJ*, 436, 599
- Tanaka, Y., Boller, T., Gallo, L., Keil, R., & Ueda, Y. 2004, *PASJ*, 56, L9
- Uttley, P., Cackett, E. M., Fabian, A. C., Kara, E., & Wilkins, D. R. 2014, *A&A Rv*, 22, 72
- Vaiana, G. S., & Rosner, R. 1978, *ARA&A*, 16, 393
- Wilkins, D. R., Cackett, E. M., Fabian, A. C., & Reynolds, C. S. 2016, *MNRAS*, 458, 200
- Wilkins, D. R., & Fabian, A. C. 2011, *MNRAS*, 414, 1269
- . 2012, *MNRAS*, 424, 1284
- Zoghbi, A., Fabian, A. C., Reynolds, C. S., & Cackett, E. M. 2012, *MNRAS*, 422, 129
- Zoghbi, A., Cackett, E. M., Reynolds, C., et al. 2014, *ApJ*, 789, 56